JOURNAL OF GEOPHYSICAL RESEARCH, VOL. 94, NO. A1, PAGES 227-240, JANUARY 1, 1989

ON THE BULK MOTION OF THE ION CLOUDS FORMED BY THE AMPTE SOLAR WIND/MAGNETOSHEATH RELEASES

Sandra C. Chapman

School of Mathematical Sciences, Queen Mary College, London

Abstract. A principal objective of the Active Magnetospheric Particle Tracer Explorers mission was to release lithium and barium ion clouds that were initially sufficiently mass dense to strongly perturb the ambient solar wind or magnetosheath flow. A key property of these release clouds was that their spatial and temporal scales were smaller than, or of the order of, the Larmor scales of all the ion species involved. A one-dimensional hybrid simulation study conducted by Chapman and Schwartz (1987) showed that momentum could be transferred locally from the oncoming protons to the majority of the release ions, which are associated with the diamagnetic cavity produced by the release, via the quasi-steady boundary layer that forms at the cavity edge. The direction of motion of these "snowploughed" release ions and the field structure that accelerates them is just that of the oncoming protons. The remainder of the release cloud is photoionized outside of the diamagnetic cavity, and as a consequence of the "pickup" interaction of these ions in the oncoming proton flow the protons are deflected from their ambient flow direction in the release cloud vicinity. This deflected direction of the oncoming proton flow, just upstream of the snowplough fields, then defines the direction of motion of the snowploughed release ions, which eventually comprise the release ion cloud that is observed from the ground. This transverse component to the direction of the release ion cloud motion suggested by the above simple picture is qualitatively consistent with ground-based observations of the barium releases. Here this simple model for the snowplough dynamics is discussed quantitatively for the particular conditions of the various lithium and barium releases. In particular, the model is found to accurately predict the time taken for the snowplough to return to the Ion Release Module (IRM) (the release spacecraft) location after the initial expansion of the cloud, an event which, as suggested from both the Chapman and Schwartz simulation results and the IRM in situ data, corresponds to the return of the magnetic field at the IRM. The magnitude of the transverse displacement of the December 27, 1984 barium release ion cloud that was seen from ground-based optical observations is also predicted by results from the simple model. Finally, the model suggests that for the barium releases, ~ 10-15% of the total number of ions released were photoionized upstream of the snowplough field structure and were therefore available to balance the transverse momentum of the snowploughed release ion cloud, via the deflected proton flow. Simple considerations suggest that this fraction should be adequate to balance the observed transverse momentum of the release ion cloud.

1. Introduction

A principal objective of the active experiments in space that were part of the Active Magnetospheric Particle Tracer Explorers (AMPTE) mission [Krimigis et al., 1982] was to release ion clouds that were sufficiently mass dense to constitute a strong perturbation to the ambient plasma flow.

Paper number 88JA03570.
0148-0227/89/88JA-03570$05.00

This was achieved by releasing slowly expanding clouds of photoionizing neutral lithium or barium from the German Ion Release Module (IRM) when it was located in the solar wind, upstream of the Earth's bow shock, or in the magnetosheath. Releases were also made in the magnetotail, but due essentially to the much lower ambient plasma flow speed they exhibit a different class of behavior and hence will not be discussed here (they have been addressed elsewhere, [e.g., Bernhardt et al., 1987]). All of the solar wind and magnetosheath releases were observed to produce qualitatively similar perturbations in the ambient field and flow, although the heavier barium, with a much shorter photoionization time (~ 30 s compared with ~ 1 hour for lithium), gave rise to a much higher initial ion mass density and hence longer-lived disturbance.

A second spacecraft, the UKS (United Kingdom Subsatellite) was located close to the IRM during the AMPTE mission. For the lithium solar wind releases, on September 11, and September 20, 1984, this separation was ~ 30-35 km, and for the first barium release, on December 20, 1984, it was ~ 170 km (the UKS was nonoperational for the magnetosheath barium release, on July 18, 1985). For all of these events, the release plasma density was sufficiently high at the IRM that the magnetic field there was seen to be supressed to zero [Lühr et al., 1986a, b] for ~ 6 s for lithium and for ~ 80 s for barium. This diamagnetic cavity did not extend to the UKS, however, giving an upper limit on the scale size of the interaction region. These spatial and temporal scales are smaller than, or of the order of, the Larmor scales of all the ion species involved in the interaction (release ions and oncoming protons) but are much larger than the Larmor scales of the electrons. A hybrid description, in which the ions are treated kinetically and the electrons are treated as a massless, charge neutralizing fluid, was therefore appropriate for a study of the interaction between the release ions and the oncoming proton flow. In order to understand the way in which momentum is transferred locally between the two ion species, a one-dimensional hybrid simulation was conducted by Chapman and Schwartz [1987]. The approach of this study differed from that of previous work, which had concentrated on the global three-dimensional aspects of the release. "Global" descriptions have been attempted from both an analytical [Haerendel et al., 1986; Papadopoulos et al., 1986; Cheng, 1987] and a numerical [Lui et al.,1986; Brecht and Thomas,1987] point of view and have in most cases been principally aimed at rationalizing the initial motion of the barium release cloud, which was deduced from ground-based observations to be transverse to the direction of the ambient flow, that is, approximately in the opposite direction of the ambient convection electric field [e.g., Valensuela et al., 1986]. The study by Chapman and Schwartz revealed details of the interaction which had not been discussed in any of these previous descriptions and as a result gave the possibility of a more detailed quantitative investigation of the release cloud motion. It is just such an investigation that will be addressed in this paper.

The results of the Chapman and Schwartz [1987] simulation showed that a well-defined, quasi-steady boundary layer evolves between the release ion population associated with the diamagnetic cavity and the oncoming proton flow. Details of the boundary layer structure are

found in the IRM in situ data, suggesting that this momentum transfer mechanism is in operation during the releases [Dunlop et al., 1987]. Essentially, the bulk of the release ions are moved en masse by a "snowplough" type process, gaining momentum from the oncoming protons which are in turn slowed by the boundary layer structure. The direction of motion of the "snowploughed" release ions is just that of the oncoming protons. It is important to note that the oncoming protons in the release vicinity have been deflected from their ambient (undisturbed) flow direction as they interact with the release ions that were created outside of the diamagnetic cavity and boundary layer region (see also Chapman and Dunlop [1986]). On the basis of the simulation results, Chapman and Schwartz [1987] developed an approximate equation of motion, which for the simple release ion density profile used in the one-dimensional simulations gave quantitative estimates of the snowplough dynamics which were in good agreement with the simulation results.

We would now like to compare the behavior that is found by integrating this approximate snowplough equation of motion with the observed global behavior of the actual releases, in order to establish whether or not the "local" momentum transfer process that was found to operate in the one-dimensional simulations, and in the in situ data, contributes substantially to the observed release cloud motion. The approximate equations of motion will first be introduced in the next section, along with details of the numerical method required for their integration. The snowplough motion depends crucially upon the number density of release ions which it encounters. In section 3 we therefore derive a simple expression for the release ion density profile, normalizing it to the single-point measurement of the ion number density as a function of time that was obtained at the IRM for each release. The results of integrating the snowplough equations with this model for the release ion density will be discussed in section 4 and compared with quantitative features of the global release ion cloud behavior. These may be obtained from the IRM in situ data, which determine the time taken for the snowploughed release ions to return to the IRM location after the initial expansion of the release cloud, and in the case of the December 27 barium release, from ground-based optical observations of the release ion cloud motion. A summary is given in section 5.

2. The Snowplough Description

Before introducing the snowplough equations of motion, we will begin by setting the essentially one-dimensional snowplough description into the context of a three-dimensional release. An attempt to do this is shown in Figure 1, which is a simplified version of Figure 7 of Chapman and Schwartz [1987]. For the purposes of future reference, the $\hat{x}'$, $\hat{y}'$, $\hat{z}'$ coordinate system of this figure has been chosen to correspond approximately to x, y, z GSE (x directed toward the Sun, z northward perpendicular to the ecliptic plane, and y completing the orthogonal set) for the particular geometry of the December 27 barium solar wind release, although the discussion to be presented here applies for all of the releases. The coordinate system in which we shall later discuss the motion of the snowplough is oriented on this diagram by the direction of motion of the snowplough itself, $\hat{x}$, that is, the direction of the oncoming disturbed proton flow $\underline{V}_{sw}$ just upstream of the snowplough boundary structure, the $\hat{y}$ and $\hat{z}$ coordinates simply completing the orthogonal set without further constraint. Figure 1 is drawn to represent only those ion populations relevant to the simple snowplough model under discussion here, so that it must be remembered that this does not include all of the detailed behavior found in the

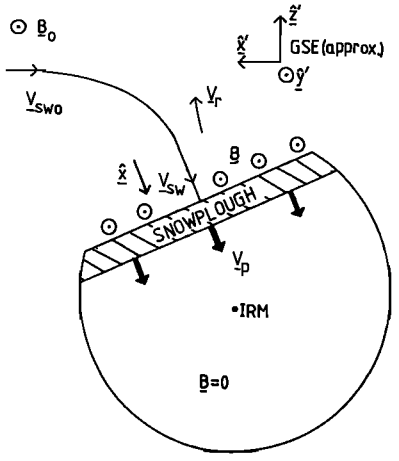

Fig. 1. This figure shows a simplified representation of the one-dimensional snowplough mechanism for the transfer of momentum between the oncoming proton flow and the release ions associated with the diamagnetic cavity (a more detailed version may be found in the work of Chapman and Schwartz, [1987]). The plane of the diagram has been chosen to be perpendicular to the ambient magnetic field $\underline{B}_o$ and to contain the IRM location (the center of the release cloud at t = 0), and hence it also contains the ambient and disturbed solar wind flow velocities $\underline{V}_{swo}$ and $\underline{V}_{sw}$, the snowplough velocity $\underline{V}_p$ and the velocity $\underline{V}_r$ of the release ions that are created upstream of the snowplough. The $\hat{x}$ axis (of the coordinate system used in the calculation of the snowplough motion) is aligned with the direction of motion of the deflected oncoming proton flow and consequently also with the direction of motion of the snowplough. The $\hat{x}'$, $\hat{y}'$, and $\hat{z}'$ axes correspond approximately to $\underline{x}$, $\underline{y}$, and $\underline{z}$ GSE for the December 27 barium release geometry, with the ambient solar wind moving in the $-\hat{x}'$ direction and the ambient magnetic field being directed approximately in the $\hat{y}'$ direction.

one-dimensional simulations. Figure 1 is drawn in the plane which contains the direction of the ambient (undisturbed) proton flow $\underline{V}_{swo}$ and the center of the release cloud at t = 0 (i.e., the IRM location, x = y = z = 0). For simplicity, the ambient magnetic field $\underline{B}_o$ is taken to be perpendicular to the plane of the diagram, so that the ambient convection electric field also lies in the plane. Since the simple two-dimensional description used here does not include mechanisms which can, on average, change the direction of the magnetic field (i.e., by "draping" around the obstacle formed by the release cloud), $\underline{B}$ always remains perpendicular to the plane. A large proportion of the release ions are assumed to be created within, and therefore associated with, the diamagnetic cavity formed during the early stages of the release, which is represented here as bounded by the solid line. The remainder of the release ions will, however, be created outside of this field free region and will begin to be picked up by the oncoming proton flow, extracting momentum from it. The macroscopic forces which act on both these release ions, and the oncoming protons in this "mass loading" region, can be shown from a multifluid description [Chapman and Dunlop, 1986; Chapman and Schwartz, 1987] to act in the local $\underline{U}_\alpha \wedge \underline{B}$ direction, where $\underline{U}_\alpha$ is just the relative velocity between a particular αth ion species and the velocity of the center of charge of the plasma as a whole. Release ions, which are created approximately at rest, i.e., with $\underline{V}_\alpha = 0$ in the oncoming solar wind flow $\underline{V} = \underline{V}_{sw}$, will have a velocity relative to the net plasma center of charge in the $-\underline{V}_{sw}$ direction and will hence move in the $-\underline{V}_{sw} \wedge \underline{B}$ direction, i.e.,

approximately in $+\hat{z}'$, or upward on Figure 1. In the "test ion" limit, i.e., far upstream, where the release ion mass density is low in comparison with that of the protons, the oncoming flow will be essentially undisturbed, with $\underline{V}_{sw} = \underline{V}_{swo}$, and the release ions just move in the direction of the ambient convection electric field $-\underline{V}_{swo} \wedge \underline{B}_o$ as defined in the rest frame of the release (i.e., exactly in $+\hat{z}'$). However, as the protons approach the cavity, they move into a region of dense, relatively slowly moving release pickup ions just outside. The addition of the slowly moving release ions to the flow effectively reduces the net center of charge velocity of the plasma, so that the protons, moving with a velocity $\sim V_{swo}$ relative to the net center of charge, experience a $\underline{U}_\alpha \wedge \underline{B} \approx \underline{V}_{swo} \wedge \underline{B}_o$ force that is directed approximately in $-\hat{z}'$, or downward on the figure, that is, in the opposite sense to that of the pickup release ions, momentum being conserved between the two species. A deflection and slowing of the oncoming ion flow that is consistent with this description has been observed in the in situ ion data for the releases [e.g., Haerendel et al., 1986], although the UKS and IRM ion instruments, which measure energy per charge, cannot be used to uniquely distinguish ion populations of different masses. Since $\underline{B}$ always remains perpendicular to the plane of the diagram, the $\underline{U}_\alpha \wedge \underline{B}$ force always acts in the plane, so that the plane also contains the velocities of the release ions and oncoming protons just upstream, or outside, of the snowplough field structure.

Understanding the ion behavior upstream of the snowplough field structures, in terms of the $\underline{U}_\alpha \wedge \underline{B}$ force, has important consequences for the global motion of the ion cloud that is acted on by the snowplough field structure. In effect, release ions created upstream locally exchange momentum with the oncoming proton flow, slowing and deflecting it as shown. The deflected protons then interact with the quasi-steady snowplough field structure that forms at the cavity boundary, transferring momentum to the snowploughed release ion population associated with it, such that the direction of motion of the snowplough $\hat{x}$ is just that of the deflected proton flow. If no other forces are present, the release ions created inside the field free region of the diamagnetic cavity only gain momentum by interacting with the snowplough field structure, so that the entire release ion cloud is eventually accelerated by being "gathered up" by the propagating snowplough fields, and becoming part of the snowploughed ion population. As the direction of motion of the snowploughed release ion cloud is just that of the deflected solar wind flow, we would expect it to be at some angle to the ambient solar wind flow direction. Whether or not this angle is sufficiently large to account for the observed transverse motion of the barium release ion clouds depends upon the fraction of release ions that are created upstream of the snowplough field structure. It is the momentum of this population which ultimately must balance the transverse momentum of the snowploughed release ion cloud, with the deflected solar wind protons just acting as an intermediary, transferring momentum between the two release ion populations.

Unfortunately, as the UKS and IRM ion experiments cannot distinguish between ion species of different masses, no exact measurement of the deflected solar wind velocity is available. Other quantitative features of the simple model of Figure 1 are directly accessible in the data however, and will be calculated by integrating the snowplough equations of motion. The time taken for the snowploughed release ions to return to the IRM location after the initial expansion of the release ion cloud can accurately be determined, as the arrival of the snowploughed ions is clearly evident in the IRM in situ data [Chapman and Schwartz, 1987]. The global motion of the release ion cloud is also approximately known from ground-based observations [Valensuela et al., 1986; Rees et al., 1986]. Finally, the integration of the snowplough equations yields the fraction of the total number of release ions which are expected to be created upstream of the snowplough field structure. This should indicate whether or not it is reasonable to expect this population to balance the transverse momentum of the snowploughed release ion cloud.

Before moving on to this detailed quantitative investigation it is perhaps worth outlining the differences between the model described here (see also Chapman and Schwartz [1987]) and those suggested by Haerendel et al. [1986] and Cheng [1987]. In those models, the strong "$\underline{U}_\alpha \wedge \underline{B}$" interaction between the oncoming protons and the release ions located outside of the cavity, which acts to deflect the oncoming proton population, is not taken into account. Asymmetry in the enhanced magnetic field surrounding the cavity and deflection of the oncoming protons in the same sense as is expected to occur from the $\underline{U}_\alpha \wedge \underline{B}$ interaction were considered by Cheng [1987] to result instead from an asymmetric space charge that builds up on the release cloud surface. The amount of transverse momentum that may be imparted to the bulk of the release ions via asymmetric charging is limited by the quantity of charge that may accumulate and hence is related to the flux of oncoming protons that impinge upon the release cloud surface, directly inducing the charge, and the ability of the ambient plasma to neutralize the charge, rather than being ultimately limited by the transverse momentum that can be carried by the release ion population that is photoionized "upstream" of the snowplough (see Figure 1), which will be estimated here. Also, the $\underline{U}_\alpha \wedge \underline{B}$ interaction, along with the snowplough boundary structure itself as envisaged here, arises under the assumption of quasi-neutrality, so that these two descriptions of events cannot be regarded as equivalent.

Alternatively, the snowplough type mechanism for momentum exchange has been assumed to simply act along the unperturbed ambient proton flow direction, ultimately resulting in the collapse of the diamagnetic cavity as seen at the IRM. The subsequent motion of this snowplough structure does not then account for the observed transverse motion of the release ion cloud as a whole. Instead, the transverse momentum of the ion cloud is balanced by that of release ions as they exit the $-\underline{V}_{swo} \wedge \underline{B}$ oriented face of the cloud. The momentum imparted to the release ion cloud by these "extracted" ions directly in this way must depend crucially upon the extracted ion momentum in the immediate vicinity of the boundary of the release ion cloud itself, as subsequently these ions can only exchange momentum with the cloud via the $\underline{U}_\alpha \wedge \underline{B}$ coupling process with the oncoming protons as described above (and by Chapman and Schwartz [1987]). Details of the mechanism for the extraction of these ions are not well known, indeed the one-dimensional field structures found by the Chapman and Schwartz simulation study act to prevent release ion migration across the boundary layer. An added mechanism not represented in the one-dimensional hybrid description, due for example to the two- to three-dimensional nature of the problem, or the presence of microinstabilities, would be required to allow ion extraction to take place. The momentum imparted by the extracted ions is hence not known explicitly. In general then, the number of extracted ions required to account for the transverse motion of the release ion cloud directly will differ from the number found to be photoionied upstream from integrating the snowplough equations as is done here, the latter population achieving momentum transfer via $\underline{U}_\alpha \wedge \underline{B}$ coupling with the oncoming protons. Calculating the number that are expected to be photoionized upstream will, in later sections of this paper, allow us to show that this release ion population is adequate to balance the transverse momentum of the

remaining population that forms the release ion cloud. Since different fractions of the total release ion population will generally be required to achieve transverse momentum balance by these two different mechanisms, the time dependent mass of the release ion cloud will also differ, along with its expected trajectory.

In conclusion, we cannot eliminate the possibility that either (or all three) mechanisms are in operation during the release events, however it will be shown here that the snowplough description (as detailed in Figure 1) can alone account for the observed quantitative features of the bulk motion of the various release ion clouds seen both in the IRM in situ data and from ground-based measurements.

2.1. The Snowplough Equations of Motion

The one-dimensional hybrid simulation study conducted by Chapman and Schwartz [1987] showed that momentum transfer between the release ions associated with the diamagnetic cavity and the oncoming proton flow could be achieved via an interaction with a propagating, quasi-steady field structure. A simple model was proposed in which the various ion populations encounter the propagating field structure (the snowplough), suffering an effective collision with it. The net result is a loss of momentum to the oncoming protons, momentum which is just ultimately transferred to the release ions that encounter the snowplough field structure as it propagates into the release cloud. Now provided that the release ion number density is such that the snowplough continually accelerates, all the release ions that have encountered it after its formation shortly after the release time (t = 0) will be continually accelerated also. The release ions will, after having encountered the snowplough, simply move with the snowplough speed V_p, effectively constituting the entire snowplough mass which continually gains momentum from the oncoming solar wind.

In this simple model, the snowplough fields act to transfer momentum along the direction of motion of the snowplough, $\hat{x}$ only (that is, in the direction of the oncoming proton flow) so that all the variables here, such as the snowplough mass per unit area M_p and speed V_p, along with the release ion expansion speed v_r (i.e. the speed of release ions which are still moving within the field free diamagnetic cavity and have not yet encountered the snowplough) are all just treated as functions of distance x and time from the release t only. The snowplough itself is hence a planar structure of infinite extent in the y and z directions, although here we essentially consider the motion of surface element in this plane dydz sufficiently small that the release ion number density n_r can be simply taken as a function of x and t, and we will examine the particular element which at some time will pass through the IRM location (i.e., y = 0, z = 0) in order to facilitate comparison with the in situ data. The rate of change of the mass of release ions moving with the snowplough at speed V_p per unit area is then given by

$$\begin{cases} \dfrac{d}{dt} M_p(x,t) = m_r n_r(x,t)(V_p(x,t) - v_r(x,t)) & V_p > v_r \\ \dfrac{dM_p(x,t)}{dt} = 0 & V_p \leq v_r \end{cases} \quad (1)$$

where m_r is the release ion mass. Implicit in (1) is that the snowplough can of course only gain mass if it is moving faster than the release ions in its vicinity that have yet to interact with it.

To a good approximation, the release ions are just created with the expansion velocity of their source neutrals, and for the purposes of this simple model we assume that the ions are not subsequently energized, except by their interaction with the snowplough or moving boundary layer field structure itself. While this is perfectly valid for those ions created within the diamagnetic cavity, where the electromagnetic fields have presumably been locally suppressed by the response of the release electron cloud, it is strictly speaking not the case for ions created in the upstream solar wind flow. For the form of the release ion cloud employed here, however these release ions, created in the oncoming solar wind flow upstream of the snowplough fields do not contribute significantly to the mass or momentum of the snowplough by directly interacting with it, instead contributing primarily to the overall global acceleration of the release ion cloud by effectively deflecting and slowing the oncoming proton flow as described in the previous section (the slowed proton flow speed then being required as a constant in the integration of the snowplough equations of motion). We therefore assume that before interacting with the snowplough, the release ions all initially move with the speeds of the neutrals that act as their source, $v_r(x,t) = x/t$ (the sign of v_r in (1) is hence just dependent upon whether the snowplough is located upstream or downstream of the release point).

An expression for the rate of change of momentum of the snowplough can be obtained as follows. An ion population, such as the oncoming solar wind protons with speed v_{sw} and constant number density n_{sw} is assumed to interact with the snowplough field structure so that the ions effectively suffer collisions with coefficient of restitution ϵ. In the frame moving with the snowplough speed V_p the ions have a velocity $-\epsilon(v_{sw} - V_p)$ after the interaction, so that their change of momentum in the rest frame (in which the solar wind proton speed is v_{sw}) is just $\Delta P_x = -(v_{sw} - V_p)(1 + \epsilon)m_p$. As the proton flux interacting with the snowplough is $n_{sw}(v_{sw} - V_p)$, momentum is delivered to the snowplough at the rate $(1 + \epsilon)m_p n_{sw}(v_{sw} - V_p)^2$. An analogous expression gives the momentum transfer rate from the release ions encountered by the snowplough. The sum of these two represents a net force acting upon the existing snowplough of mass M_p per unit area. Assuming that the release ions that have interacted with the snowplough always subsequently move with it at the snowplough speed, so that they interact with a coefficient of restitution $\epsilon = 0$, conservation of momentum between the snowplough and the interacting protons and release ions gives

$$M_p(x,t)\frac{d\,V_p(x,t)}{dt} = (1 + \epsilon)n_{sw}m_p[v_{sw} - V_p(x,t)]^2 - m_r n_r(x,t)[v_r(x,t) - V_p(x,t)]^2 \quad (2)$$

which, along with

$$\frac{dx(t)}{dt} = V_p(x,t) \quad (3)$$

and equation (1), completely specifies the snowplough motion. In the results to be discussed later in this paper we will assume that $\epsilon = 0$ for the oncoming protons, as well as the release ions. This value is suggested by the boundary layer simulation results [Chapman and Schwartz,

1987], although in principle a different or varying value of ϵ for the protons could be chosen.

The contribution of the proton mass to the total mass per unit area M_p of the snowplough has also been neglected in comparison with that of the release ions. This assumption is reasonable if we consider that for a barium release, for example, the region on which the diamagnetic cavity extends is known to be limited by the UKS–IRM separation and is ~ 100 km. Since the release event is seen from optical observations to be τ ~ 400 s in duration, the mass of solar wind protons that have impinged on this region of area A ~ 100 km^2 is approximately $v_{sw}\tau A n_{sw} m_p \sim 10^{25}$ m_p. This must be compared with the mass of released photoionized barium, ~ 137 times (a few) times 10^{24}–10^{25} m_p, which is expected to be mostly gathered up by the snowplough. A similar calculation for the lithium releases shows that the solar wind mass that would have been expected to accumulate at the snowplough from our simple picture would represent an even smaller fraction of the total snowplough mass.

2.2. Integration of the Snowplough Equations of Motion

Equations (1) to (3) have been integrated using a fourth–order Runge Kutte scheme with variable time step, the time step being sufficiently small that the numerical errors accumulated over an entire integration (i.e., over a time greater than the time scale of the event) are < 0.3% (confirmed by progressively reducing the time step for several sample snowplough integrations performed over the range of parameter space).

The initial conditions for the integration are chosen to reflect features of the snowplough structure formation seen in the boundary layer simulation results of Chapman and Schwartz [1987]. These and further simulations over a range of different release ion masses suggest that the formation time of the snowplough field structure is ~ 0.5–1 s for lithium and up to a few seconds for barium, which for the latter is short compared with the ~ 80 s over which the diamagnetic cavity persists at the IRM for the barium release. This time scale does represent a larger fraction of the ~ 6 s for which the magnetic field is zero at the IRM in the case of the lithium releases, so that we might expect quantitative results obtained from integrating the snowplough equations to compare less favorably with the corresponding observations in these cases. The snowplough itself is taken to be initially at rest and at a distance from the release cloud center where the release ion number density is just sufficiently large to be represented computationally. An arbitrarily small but nonzero initial snowplough mass per unit area is also required as an initial condition, in order to allow integration of (2). In the sample results to be discussed here the initial mass $M_o = 10^4\ n_{sw} m_r$ kg m^{-2} (n_{sw} and m_r in SI units), or 0.1 $n_{sw} m_r L_o$ where L_o = 100 km, a typical estimate of the scale size of the barium release cloud. This value for M_o is found to be reasonable, as it represents a negligibly small fraction of the typical mass per unit area of the snowplough at later times.

To ensure that the above initial conditions do not dictate the properties of the subsequent snowplough behavior, the integration was repeated over a substantial range of initial conditions. For a barium release, it is then found that if the start time of the integration t_o was varied from 0.1 to 10 s, a change of only 3% is produced in the snowplough parameters at the time when the snowplough returns to the IRM, for example, ~ 80 s later (t_o = 1 s was used to produce the results to be presented here). In the case of a lithium release however, a similar variation in t_o of 0.05–1 s yields a variation of ~ 20% in the time (approximately a few seconds) that the snowplough is calculated to take to return to the IRM, with a smaller variation in all other parameters (in this case t_o = 0.5 is used). On varying the initial snowplough mass from 0.01 to 1.0 $n_{sw} m_r L_o$ it is found that all snowplough parameters vary by < 3% at all later times of interest here, for all of the releases. The initial location and speed of the snowplough can also be varied over several orders of magnitude to yield negligibly small differences in the calculated snowplough motion after an initial transient phase of less than 1 s duration. In particular, values of the initial snowplough speed were varied from that of the local release ion speed v_r (a few kilometers per second) to the oncoming solar wind speed v_{sw} (a few hundred kilometers per second). In summary then, the results to be presented here may, as far as the integration procedure is concerned, be considered to be accurate to within a few percent for the barium releases and to within ~ 20% for the lithium releases.

In order to integrate equations (1)–(3) we finally require values for the number densities and initial velocities of the solar wind and release ion populations. In the model used here, release ions that are created outside the cavity, in the oncoming proton flow, are expected to be accelerated, causing the protons to deflect and decelerate in order to conserve momentum. As no direct measurement of the disturbed solar wind velocity and number density in the vicinity of the release ion cloud is available as required, the snowplough equations of motion will be integrated using constant values for the solar wind speed and number density, and in section 4 we will examine the significance of choosing different values for these parameters. It just remains to specify the release ion number density profile to be used in the integration in the following section.

3. The Ion Number Density Function

We will now obtain a simple expression for the release ion number density distribution function $n_r(\underline{r},\underline{v},t)$ within the diamagnetic cavity. First, a functional form of the density distribution function will be derived analytically from simple considerations concerning the properties of the release clouds. This functional form will of course depend upon a number of parameters which characterize each release, such as the mean expansion velocity of the released neutrals that act as a source for the ions, the total number released, and their photoionization time scale. In situ IRM measurements of the ion density as a function of time at a single point in space will then be used to normalize the simple expression for the density distribution function, partially constraining these parameters.

The release clouds of barium or lithium vapor become collision free almost immediately after exiting the release canisters (i.e., within ~ ½ s, the total time taken for the release reaction (G. Haerendel, private communication, 1986)). The neutral density is sufficiently high that photoionization produces electron number densities that are large enough to locally support a diamagnetic cavity, suppressing the ambient electric and magnetic fields to zero. Also, the photoionization process is such that the initial ion velocities are just those of their source neutrals, to a good approximation. Within the cavity then, both ions and neutrals move on straight line trajectories, their phase space coordinates at the "release time", $\underline{r}_o$, $\underline{v}_o$, t_o = 0 (i.e., when the cloud becomes collision free), being related to those at some time later, $\underline{r}$, $\underline{v}$, t, by $\underline{v}_o = \underline{v}$ and $\underline{r}_o = \underline{r} - \underline{v}t$. The distribution function of the particles at t_o = 0, $f_{tot}(\underline{r}_o,\underline{v}_o,0)$ determines it along these phase space trajectories at any later time. Here, at t_o = 0 the particle

distribution function is taken for simplicity to have the following form:

$$f_{tot}(\underline{r}_o,\underline{v}_o,0) = \frac{K}{v_{tx}\, v_{ty}\, v_{tz}\, R_x\, R_y\, R_z} \qquad (4)$$

$$.\exp -\left[\frac{x_o^2}{R_x^2} + \frac{y_o^2}{R_y^2} + \frac{z_o^2}{R_z^2}\right] \exp -\left[\frac{v_{xo}^2}{v_{tx}^2} + \frac{v_{yo}^2}{v_{ty}^2} + \frac{v_{zo}^2}{v_{tz}^2}\right]$$

The release particle cloud distribution is just Gaussian in form in both real and velocity space, with different mean velocities v_{tx}, v_{ty}, v_{tz}, and mean spatial extent R_x, R_y, R_z in the three Cartesian directions. The denominator of (4) represents the mean volume in phase space occupied by the release cloud. By Liouville's theorem, the distribution function at some later time t along the phase space trajectories $f_{tot}(\underline{r},\underline{v},t) = f_{tot}(\underline{r}_o,\underline{v}_o,0)$ and normalizing to determine the arbitrary constant K finally yields

$$f_{tot}(x,y,z,t) = \frac{1}{\pi\sqrt{\pi}} \frac{\exp -\left[\frac{x^2}{R_x^2 + v_{tx}^2 t^2}\right]}{(R_x^2 + v_{tx}^2 t^2)^{\frac{1}{2}}} \qquad (5)$$

$$\exp -\left[\frac{y^2}{R_y^2 + v_{ty}^2 t^2}\right] \exp -\left[\frac{z^2}{R_z^2 + v_{tz}^2 t^2}\right]$$

$$. \frac{}{(R_y^2 + v_{ty}^2 t^2)^{\frac{1}{2}}} \frac{}{(R_z^2 + v_{tz}^2 t^2)^{\frac{1}{2}}}$$

This does not, of course, represent a unique choice for f_{tot}, the only constraint on the chosen function being its integrability over phase space in order to normalize for K. The total number of released neutrals just decreases exponentially by photoionization, with a time constant τ_p. If the total number of release particles is N_o, then the ion density distribution becomes

$$n_r(x,y,z,t) = N_o\,(1 - e^{-t/\tau_p})\, f_{tot}(x,y,z,t) \qquad (6)$$

Now, since the release is made from two canisters, which prior to ignition have drifted some distance from the IRM in some unknown direction, we can take the initial spatial scale of the cloud to be dominated by this canister separation, R, i.e., $R_x \sim R_y \sim R_z \sim R$. These initial release cloud dimensions will be significant for times $t \sim R_x/v_{tx}$, etc., the cloud at later times behaving as if it originated from a single point in space ($R \to 0$). One further possible feature of the behavior of the release particle cloud is that it drifts as a whole with respect to the release point. A drift of the order of the mean expansion speeds of the particles was observed in the case of the first barium release [Rees et al., 1986]; this might be expected to be a nonnegligible factor in the particle distribution function. Assuming for simplicity that the center of the Gaussian distribution drifts with respect to the location of its center at t = 0 (i.e., the IRM location) in the $+\hat{x}$ direction at constant speed v_d, we need only replace x by $x - v_d t$ in (5). In other words, the ion density measured at the IRM location x = 0 is just that of the ions moving with velocity $-v_d\hat{x}$.

We now wish to compare this model for the ion density distribution with in situ measurements, in order to determine reasonable values for the parameters by which the release cloud is scaled. The only measurements available inside the field free region of the diamagnetic cavity are of course those of the IRM, giving a single-point measurement of the ion number density as a function of time. No distinction can therefore be made between the different expansion speeds in different directions, so we take $v_{tx} \sim v_{ty} \sim v_{tz} = \bar{v}$. The single-point measurement also does not determine the direction of the drift velocity of the cloud as a whole. For simplicity we restrict our attention here to a single case where the trajectory of the snowplough element under consideration intersects the release ion cloud center, i.e., where the cloud drift is in the $\hat{x}$ direction only, consistent with the observations of Rees et al. [1986]. It will be shown that no further details in the model for the release cloud need to be introduced in order to obtain a good agreement between the results of integrating the snowplough equations and the observations, so that we are justified in the above simplifying assumptions concerning the release cloud geometry. The release ion number density function is finally

$$n_r(x,y,z,t) = \frac{N_o}{\pi\sqrt{\pi}} \frac{(1 - e^{-t/\tau_p})}{(R^2 + \bar{v}^2 t^2)^{3/2}} \qquad (7)$$

$$.\exp -\left[\frac{x^2}{R^2 + \bar{v}^2 t^2}\right] \exp -\left[\frac{y^2}{R^2 + \bar{v}^2 t^2}\right] \exp -\left[\frac{z^2}{R^2 + \bar{v}^2 t^2}\right]$$

with the IRM location at x = y = z = 0. The IRM ion density measurements to be discussed here are inferred from measurements of the electron plasma frequency [Gurnett et al., 1986a, b];(R. Treumann, private communication, 1987). This allows an accurate determination of the density of a singly ionized ion population which is at sufficiently low energies to fall below the range of the ion instrument on board the IRM.

This model for the expanding ion cloud then is a function of parameters N_o, τ_p, $\bar{v}$, v_d, and R, all of which are only known approximately, for example from considerations made prior to release [Haerendel et al., 1985]. Also, since we have introduced an asymmetry in the model by allowing for a nonzero cloud drift speed relative to the IRM, the single-point measurement of the ion number density at the IRM as a function of time is insufficient to uniquely determine a single set of parameters that constitute a best fit to the IRM data. The simplest possible approach, employed here, is to fit the ion number density at the IRM location as a function of time, as determined from (7), to the IRM data by minimizing with respect to a single parameter, the total number of neutrals N_o released, keeping the other parameters fixed. We can then directly compare different density versus time curves generated in this way, each curve corresponding to a different choice of τ_p, $\bar{v}$, v_d, and R, with the IRM data directly. This will then determine whether or not the chosen model (7) is adequate to describe the slow expansion phase of the release cloud, as seen by the IRM, given the expectations for the values of the various parameters involved, as well as effectively allowing us to calculate N_o as a function of these parameters.

The deviation of the fitted curve $n_r(t)$ (i.e., equation (7)) from the set of ion density measurements $n_i(t_i)$ is just

$$\Delta = \sum_i [n_i(t_i) - n_r(t_i)]^2 \qquad (8)$$

where t_i is the time when the ith measurement is made. Putting $\partial\Delta/\partial N_o = 0$ then yields an expression for the value of N_o required for the fitted curve

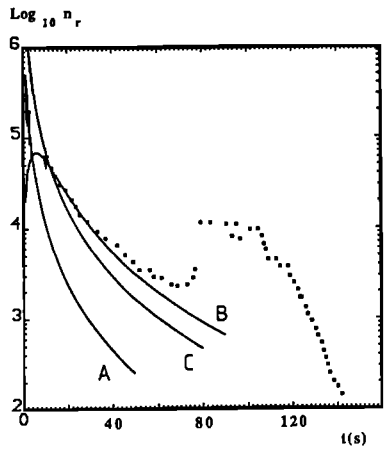

Fig. 2. This figure shows a comparison between the release ion number density seen at the IRM as a function of time marked by the dots [from Gurnett et al., 1986b], with fitted curves of the form given by equation (10) in the text. The data is for the December 27 barium release, and the first point used in each fit is marked by a triangle. The fitted curves A and B correspond to values of R of 1 and 10 km, respectively, both having been calculated using different subsets of the data consistent with equation (10), (see text), the curve C corresponding to R = 1 km, but using the same subset of the data as the R = 10 km curve B for the purpose of comparison. All curves have been calculated for typical values of the remaining parameters $\bar{v}$ = 1 km s^{-1} and v_d = 0.4 km s^{-1}. The values of N_o and σ_n/n appropriate to each curve are given on the right hand side of the plot.

$$N_o = \frac{\sum_i n_i(t_i) f_i(t_i)}{\sum_i f_i^2(t_i)} \qquad (9)$$

where $f_i(t_i) = n_r(t_i)/N_o$ and from (7) is independent of N_o. It is easily shown that $\partial^2\Delta/\partial N_o^2 > 0$ in general, so that (9) yields a value of N_o that will always correspond to a minimum in Δ between the fitted $n_r(t)$ curve and the set of data points. For the purposes of comparison, we will calculate a normalized "root mean square" deviation for each curve

$$\frac{\sigma_n}{n} = \frac{\{\sum_i [n_i(t_i) - n_r(t_i)]^2\}^{\frac{1}{2}}}{\sum_i n_i(t_i)} \qquad (10)$$

An example of the variation of the ion density at the IRM is shown in Figure 2 for the case of the first barium release. Here, the dots denote the discrete set of density measurements $n_i(t_i)$ (in cm^{-3}) plotted versus time (in seconds), and the solid lines represent curves $n_r(t)$ (given by (7) and (9)) fitted to this data set. The release time corresponds to t = 0 on the plot. After the release, the measured density first falls away due to the expansion of the release cloud within the diamagnetic cavity. This behavior continues until t ≈ 77 s, when the density rises sharply; this coincides with the return of the magnetic field at the IRM and hence corresponds to the arrival of the snowplough field structure and associated release ions at the IRM location, as described by Chapman and Schwartz [1987]. Our model for the number density function of the expanding ion cloud only applies to measurements made before this time, subsequent measurements being discarded from the data set $n_i(t_i)$ used to fit the curves and determine N_o. The curves shown in Figure 2 have been drawn for two different values of the initial cloud scale size R, and for typical values of the other parameters ($\bar{v}$ = 1.0 km s^{-1}, v_d = 0.4 km s^{-1}). On the right-hand side of the plot the appropriate values for N_o and σ_n/n are given for each curve. Curves A and B correspond to values of R = 1 and 10 km, respectively, each curve being produced from the interval of IRM data $n_i(t_i)$ that starts at the earliest possible time $t_1 = t_i > R/\bar{v}$, as we would not expect (7) to provide a good description at earlier times (the earliest data points in time t_1 used to produce these fits are marked by triangles). For the purposes of comparison, a third curve, C, has been plotted for R = 1 km, but using the same data set (i.e., the same value for t_1) as for the R = 10 km curve, B.

In general the fitted curves found for reasonable ranges of the drift and expansion speeds do not vary strongly in shape or accuracy of fit. For example, over a range of $\bar{v}$ = 0.5–1.5 km s^{-1} the deviation σ_n/n varies by ~ 5%, and over a range of v_d = 0–1.0 km s^{-1} σ_n/n varies by less than ~ 3% for the example shown. However, these fitted curves require values of N_o which do vary significantly with $\bar{v}$ and v_d, and this must then be taken into account in the calculation of the snowplough motion. For example, for curves such as B, N_o varies by approximately a factor of 5 in total over the above ranges in $\bar{v}$ and v_d. This range of v_d has been chosen to include the optical measurement of ~ 0.7 km s^{-1} for this event [Rees et al., 1986], and the range of expansion speeds includes the expected value of ~ 1 km s^{-1} (the thermal speed of the neutrals) and values implied by the optical measurements of the expansion of the release cloud of ~ 1.35 km s^{-1} [Valensuela et al., 1986] and ~ 1.5 km s^{-1} [Rees et al., 1986]. It is only the choice of the photoionization time scale τ_p that is not expected to strongly affect the calculation of the snowplough motion. Both σ_n/n and the appropriate value of N_o vary by less than ~ 18% over the possible range τ_p = 28 ± 6 s [Carlsten, 1975] in the case of a barium release. For the lithium releases the effect of varying the photoionization time will clearly be negligible in (7), since the cavity lifetime t ~ 10 s << τ_p ~ 1 hour, and this is also found to be the case. Throughout this discussion we therefore neglect the uncertainty in the photoionization time scales and simply take τ_p = 28 s and 1 hour for the barium and lithium releases, respectively.

All that remains is to examine the behavior of the fitted curves $n_r(t)$ as the initial scale size R is varied. On comparing the two curves A and B plotted in Figure 2 that refer to values of R = 1 and 10 km (and the earliest possible initial times t_1 consistent with the assumptions implicit in (7)), it is immediately clear that a good agreement with the IRM data is obtained for the R = 10 km curve. This choice of R = 10 km then represents the closest fit to the data, yielding the smallest value of the normalized deviation σ_n/n < 2% that can be obtained for any R.

As the fitted curves are obtained by minimizing the linear deviation Δ (8), achieved by simply allowing a factor in (7), i.e., N_o, to vary, it is clear that data points at earlier times on the plot, where the ion number density is largest, will dominate the properties of the fitted curve. Hence by treating t_1 as a free parameter, different curves can be obtained for any given value of R. We must therefore ensure that the "best fit" properties of the release ion clouds that are deduced by the fitting procedure described above are not sensitive to any restrictions that are imposed upon the selection of the time t_1 at which the data set used to fit the curves begins. To this end, curve C has been plotted in Figure 2, which was calculated for R

= 1 km but with the same data set as the R = 10 km curve B, that is, with the same value for t_1. This choice of t_1 for the R = 1 km curve C now yields a closer fit to the data than the R = 1 km curve A, with $\sigma_n/n \sim 8\%$. The best possible fit that can be obtained for the R = 1 km curve requires an even later time t_1 than for curve C, and although it has a deviation $\sigma_n/n \sim 5\%$ approaching that of the R = 10 km best fit shown on the figure, it represents overall a less satisfactory fit in that it applies to a smaller subset of the data points. The above suggestion that the R = 10 km curve B provides the best fit to the data set is therefore not affected by the sensitivity of the fitted curves to the earliest data points in time. The best fit curves for the remaining releases to be discussed below, all calculated using the earliest $t_1 = t_i > R/\bar{v}$, have also been found to be appropriate in this respect, yielding σ_n/n values that are either smaller than, or indistinguishable from, those of best fit curves that are produced using other arbitrary (but in all cases later) values of t_1. We are therefore justified in restricting our attention to fitted curves calculated using the earliest possible $t_1 = t_i > R/\bar{v}$, i.e., which apply to the largest possible fraction of the data set and which are consistent with the derived expression for n_r (equation (7)).

Before release it was expected that the separation of the two release canisters, which the scale length R presumably represents, would be smaller, that is, approximately a few kilometers [Haerendel et al., 1985], although the separation is not well known. As might be expected from the plot, using R = 1 km yields a poorer agreement between the model and the data, i.e., for curve A, $\sigma_n/n \sim 17\%$. The value for the total number of released neutrals N_0 that is calculated for the R = 10 km curve, $\sim 3.3 \times 10^{24}$ compares favorably with prerelease expectations of $\sim 3.4 \times 10^{24}$ [Haerendel et al., 1985], whereas the value of N_0 for the R = 1 km curve A is smaller than this by over a factor of 10. This difference in N_0 would be expected to significantly affect any quantitative properties of the snowplough motion deduced from the fitted model for the ion number density. If, as appears here the model for n_r using larger values of R provides a more accurate representation of the initial release ion cloud expansion, it would also be expected to ultimately lead to qualitative predictions of the snowplough behavior which agree more closely with observations. In the next section, the snowplough motion will therefore be calculated using both values of R, i.e., the "expected" value of 1 km and the best fit value of 10 km, to specify the appropriate value of N_0.

The best fit R, corresponding to the smallest value of σ_n/n, has been deduced for both the lithium and barium releases and is given in Table 1 for reference. In this table the best fit and R = 1 curves are compared by listing the values of the percentage normalized deviation σ_n/n and the appropriate values for N_0. From the table we can see that for the lithium releases, the best fit values of R are approximately a few kilometers, which, along with the corresponding values for N_0, are consistent with prerelease expectations. However, it must be noted that due to the shorter time scales of the lithium release events, fewer data points, i.e.~ 5-8, are available for fitting these curves, leading to larger errors in the best fit parameters. For the second barium release, parameter values for R = 10 km, rather than the best fit values have been given. In order to fit a function which is only valid for times after $R \sim \bar{v}t$, the first few points of the IRM data set that in reality starts close to t = 0 have been discarded. The fitting procedure is therefore only meaningful if this represents a small fraction of the data set and hence becomes less appropriate as R increases. In the case of the second barium release, no distinct minimum in σ_n/n is found with changing R, even up to R = 20 km, requiring ~ 15% of the data set to be discarded. However, from the table it is clear that both R = 10 km and R = 20 km correspond to values of N_0 consistent with expectations, whereas R = 1 km does not, so that given expectations also concerning R, it would seem that R = 10 km probably represents the most reasonable choice for this parameter.

4. Integrating the Snowplough Equations: Results

Having established a function for the release ion number density n_r consistent with the IRM in situ data, the snowplough equations of motion derived in section 2 can be integrated for the particular conditions appropriate for the various AMPTE solar wind and magnetosheath releases. This calculation then yields quantitative predictions for the global release behavior that can then be compared with observations. In this way we shall establish in this section whether or not the simple model for the release ion cloud motion that was proposed in section 2 is quantitatively consistent with what can be inferred about this global motion from both the in situ IRM and ground-based optical measurements.

4.1. Comparison With In Situ IRM Measurements

In the preceding discussion it has been demonstrated that the chosen function for n_r (equation (7)) is consistent with the in situ observations of the IRM for a range of values of the drift and mean expansion speeds v_d and $\bar{v}$ of the ion cloud, given the corresponding values for the total number of neutrals N_0 (from equation (9)). Quantitative aspects of the snowplough dynamics, deduced by integrating the snowplough equations of motion, are therefore expected to vary with the expansion and drift speeds of the ion cloud, so that we will present results calculated over a range of these values. It was also found that the implied initial spatial dimensions of the cloud R, which give the best agreement between the model (equation (7)) and the IRM in situ data, are somewhat larger than the spatial separation of the release canisters that was expected at the time of release, at least in the case of the barium releases.

TABLE 1. Comparison of Parameters for Best Fit and R = 1 Curves

	Typical Fit		Best Fit			R = 1 km Fit	
Release Event	$\bar{v}$, km s^{-1}	v_d, km s^{-1}	R, km	σ_n/n, %	N_0, $\times 10^{24}$	σ_n/n, %	N_0, $\times 10^{24}$
Lithium, September 11, 1984	2.5	0	4	1.7	7.2	5.3	4
Lithium, September 20, 1984	2.5	0	1			8.9	6.7
Barium, December 27, 1984	1.	0.4	10	1.5	3.3	17.4	0.24
Barium, July 18, 1984	1.	0	10*	4.6	2.2	4.3	0.49
			20*	2.6	3.8		

*Not the best fit values (see text).

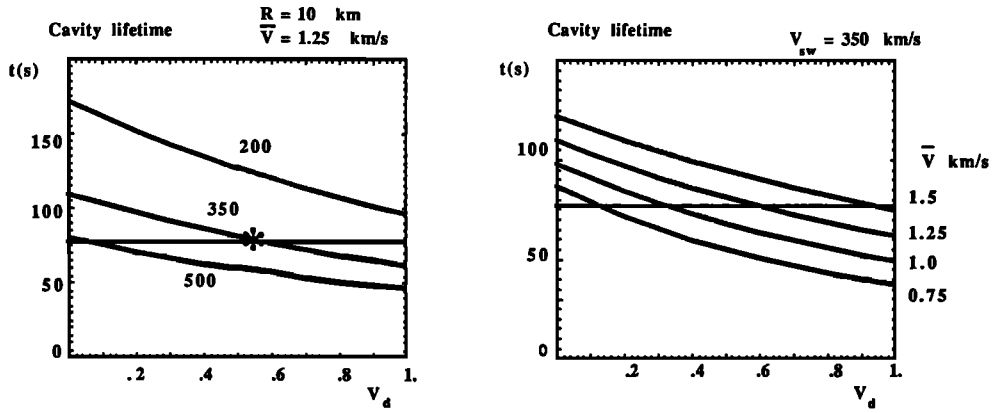

Fig. 3. (Left) A plot of the cavity lifetime at the IRM location versus the drift speed of the ion cloud v_d. The three curves show the results of integrating the snowplough equations of motion for the December 27 barium release for three different values of the oncoming proton flow speed. The plot is drawn for the best fit value R = 10 km and the typical expansion speed $\bar{v}$ = 1.25 km s^{-1}. (Right) This plot has the same axes as the left hand plot, but the four curves are instead drawn for four different values of the expansion speed and for a typical value of the oncoming proton flow speed of 350 km s^{-1}. The observed cavity lifetime is marked by the thick horizontal line in both plots.

Results will therefore be presented here for the barium releases taking both the best fit value, R ~ 10 km, and the value expected prior to release, R ~ 1 km, in turn. One further parameter which is not well known is the velocity of the oncoming solar wind protons which act as a source of momentum for the snowploughed release ions. It may be remembered that due to the creation of release ions outside of the diamagnetic cavity boundary, the ambient flow is expected to be disturbed before reaching the cavity boundary where the snowplough field structures have formed. The appropriate value for the oncoming proton flow velocity here is hence that just upstream of the snowplough field structures, rather than that of the ambient flow. We will proceed here by considering a range of values for the oncoming proton flow velocities that are suggested by (but not directly deducible from) in situ measurements from the ion instruments on board the UKS and IRM for the various release events, the maximum in this range being just that of the ambient (undisturbed) proton flow.

In comparing the snowplough motion that is determined by integration of the approximate equations given in section 2 with the in situ observations of the IRM (and with ground-based optical observations), we simply assume here that the motion of the entire release ion cloud may be interpreted as a result of the cavity-associated ions being gathered up by the moving snowplough field structure, as detailed in Figure 1. The in situ IRM observation of the snowplough motion will be a temporal one, in that the lifetime of the diamagnetic cavity as determined by the IRM will just correspond to the time taken for the snowploughed release ions to return to the IRM location after the initial expansion of the cavity. This initial expansion is modeled by the snowplough equations of motion here as simply the phase in the snowplough motion when the momentum flux of the release ions striking the snowplough is sufficiently large that the snowplough is forced to move against the direction of the oncoming proton flow (i.e., before the release ion cloud has expanded substantially). We will begin by comparing predicted cavity lifetimes determined by integrating the snowplough equations of motion for the particular conditions appropriate for the various releases with the cavity lifetimes seen at the IRM.

An attempt at such a comparison is shown in Figure 3, which displays the results of a series of integrations performed over a range of the ion cloud drift and expansion speeds, and the speed of the oncoming protons, for the December 27 barium release. The cavity lifetime, that is, the time taken for the snowplough to return to the

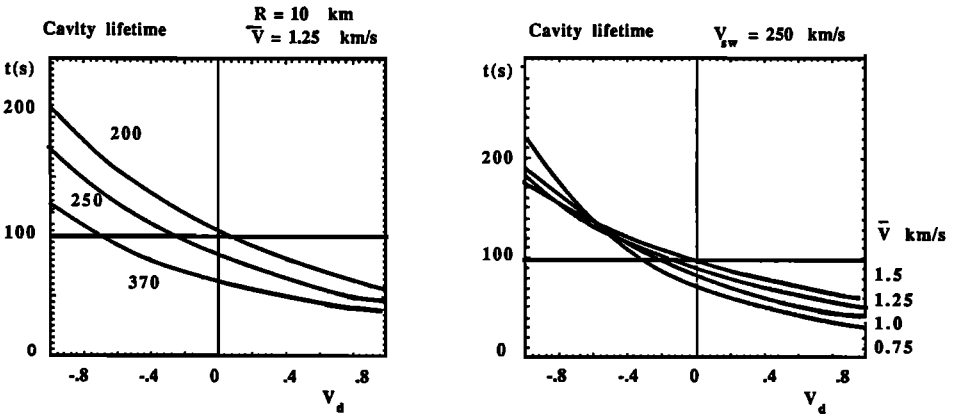

Fig. 4. This figure has the same format as Figure 3 but is drawn for the July 18 barium release with the best fit value R = 10 km.

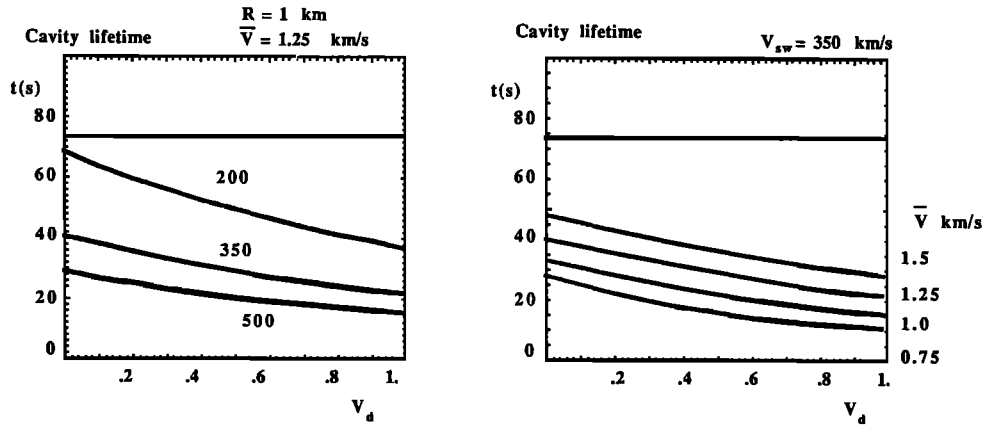

Fig. 5. This figure is in the same format as Figure 3 and refers to the December 27 barium release for R = 1 km.

IRM location, is plotted on the ordinates of the two panels, with the range of values of the ion cloud drift speed v_d along the abscissae. In the left-hand panel, the three curves have been produced for three values of the oncoming solar wind proton speed and a single typical value of the mean expansion speed $\bar{v}$ = 1.25 km s^{-1}. These values for the solar wind speed then range from the ambient value of ~ 500 km s^{-1} to values suggested by the in situ ion data for the event [e.g., Haerendel et al., 1986]. The four curves shown in the right-hand panel have been produced for a typical value of the disturbed solar wind flow speed v_{sw} = 350 km s^{-1} (which is also featured in the left-hand plot) and correspond to four values for the mean expansion speed that include both prerelease expectations for $\bar{v}$ and values suggested by the optical observations. All of the curves are determined using the best fit value for the initial cloud size R = 10 km. Given some expectations or measurements of the range in which $\bar{v}$, v_d, and v_{sw} lie, the figure provides a prediction of the cavity lifetime as seen at the IRM location. The actual cavity lifetime for this event is denoted by the thick horizontal line on both panels. Given then that the drift speed is approximately a few times 0.1 km s^{-1} for this event (i.e., ~ 0.7 km s^{-1} [Rees et al., 1985]) and that the expansion speed lies within the given range (i.e., from ~ 1 km s^{-1} [Haerendel et al., 1985] to ~ 1.25 km s^{-1} [Valensuela et al., 1986]), the predictions obtained from the simple snowplough model are in excellent agreement with the IRM measurement. The same procedure has been repeated for the July 18 barium release in the magnetosheath, and the results are shown in Figure 4. The format of Figure 4 is identical to that of the previous figure, except that since no optical observations are as yet available in a form that will allow the ion cloud drift (if any) to be determined, values of the cavity lifetime have been plotted for both positive and negative values of v_d, the magnitude of this range being of the order of that of the first barium release, since these would be expected to be similar, being produced by what should be an identical release process. Once again, the best fit value of R = 10 km has been used to generate the plot. Given that the mean expansion speed in this case is also similar to that of the first barium release, which is reasonable if, as assumed here, the principal acceleration mechanism is that of the snowplough field structure, we also find that the predicted cavity lifetime is consistent with that seen at the IRM.

The effect of varying the initial spatial extent of the ion cloud on these results, all other parameters being kept constant, is illustrated in Figures 5 and 6, where the calculated cavity lifetimes have been plotted in the same format as in the previous figures and refer once again to the December 27 and July 18 barium releases, respectively. The ion release cloud distribution functions used to produce these plots are taken to have an initial spatial extent R = 1 km, which would be consistent with prerelease expectations but which does not provide the best agreement between the model for the release ion cloud number density function n_r (equation (7)) and the in situ IRM data, as shown in the previous section. We might therefore

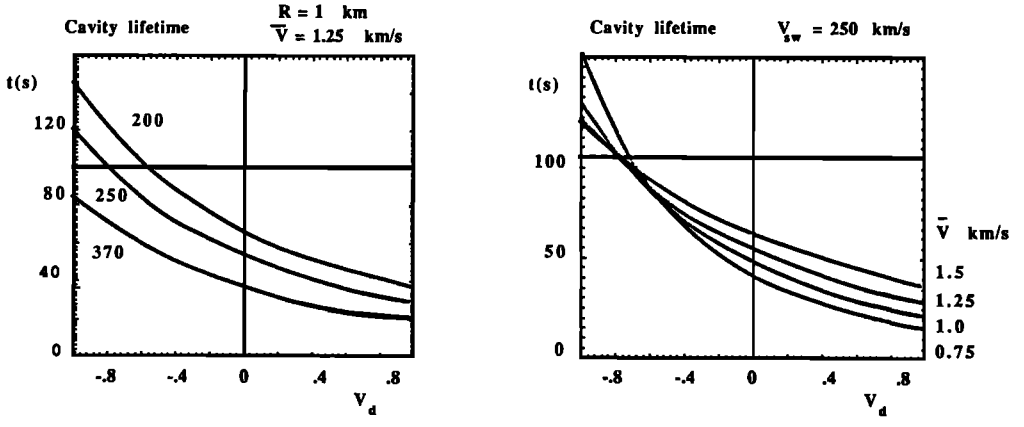

Fig. 6. This figure is in the same format as Figure 3 and refers to the July 18 barium release with R = 1 km.

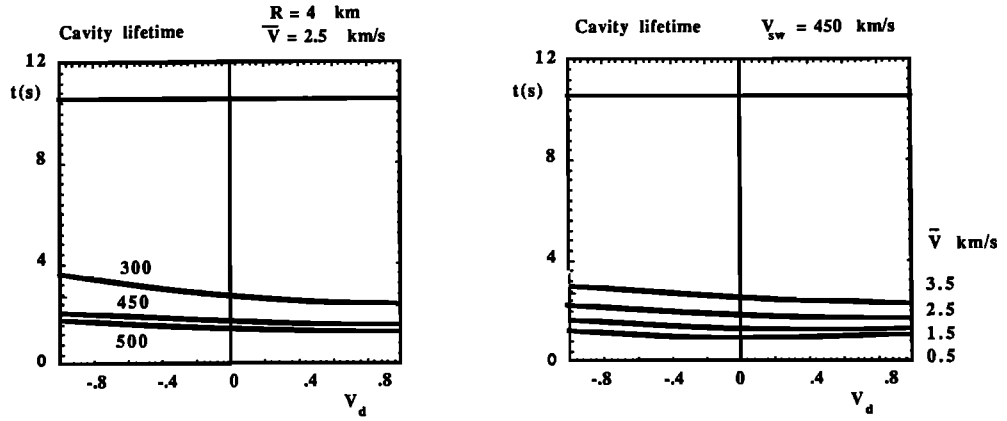

Fig. 7. This figure is in the same format as Figure 3 and refers to the September 11 lithium release.

expect that the R = 1 km curves will not be in as good agreement with the IRM in situ measurements of the cavity lifetimes as the best fit curves shown in Figures 3 and 4, and for the first barium release this is clearly the case (the predicted cavity lifetimes now being too short by about a factor of 2). For the July 18 release, however, it is still possible that the cavity lifetime measured at the IRM lies within the expected range of the parameters $\bar{v}$, v_d, and the oncoming flow speed, principally because in this case v_d is less well known, so that the range of this parameter is larger. Our conclusion here is then that although the different values for the expected and the best fit values of R imply values for the total number of neutrals that range over an order of magnitude for the December 27 release, and about half an order of magnitude for the July 18 release, the corresponding values for the cavity lifetimes vary much less. Therefore, despite this discrepancy between the expected and the best fit values of R, we are still able to provide predictions for the cavity lifetimes which are reasonably consistent with the IRM measurements, to within the uncertainties of the various parameters which characterize each release.

We can now turn to consider the case of the September 11 and 20 lithium releases, both of which took place in the solar wind. Since the best fit values of R for these releases are quite close to that expected prior to release (see Table 1), the cavity lifetimes that are found in both cases for each release are rather similar. We therefore confine our attention here to the results obtained using the best fit values of R, and these are shown in Figures 7 and 8 in the same format as the previous figures. In interpreting these plots, it must be remembered that the calculation of the snowplough motion for the lithium releases is subject to much larger errors than in the case of the barium releases, the principal sources of error being the sensitivity of the results to the initial conditions as described in section 2 and the limited number of IRM ion number density data points $n_i(t_i)$ that are available for the fitting procedure described in the last section, leading essentially to an error in the total number of neutrals N_O. It is therefore not surprising that the cavity lifetimes predicted by integrating the snowplough equations of motion are not in as good agreement with the IRM in situ measurements for the lithium releases, being in general too small by a factor of 3.

4.2. Comparison With Ground-Based Optical Observations

The other set of measurements that are available for comparison with the predictions of the snowplough equations are the ground-based optical observations of the December 27 barium release, which show the motion of the entire release ion cloud in the plane of the night sky. As this release was performed at the flank of the magnetosphere, this plane contains the ambient solar wind flow and convection electric field, to a good approximation (i.e., to within ~ 30°), and therefore the observed ion cloud motion also just lies approximately in the plane in which Figure 1 is drawn. The $\hat{x}'$, $\hat{y}'$, and $\hat{z}'$ axes of Figure 1 therefore are equivalent to $\underline{x}$, $\underline{y}$, and $\underline{z}$ GSE to within ~ 30° also. The release ion cloud produced during the July 18 event was also observed to behave in a manner similar to the December 27 release, that is, to move initially transverse to the ambient flow direction $\underline{V}$, i.e. in ~ $\underline{V} \wedge \underline{B}$ direction (M.

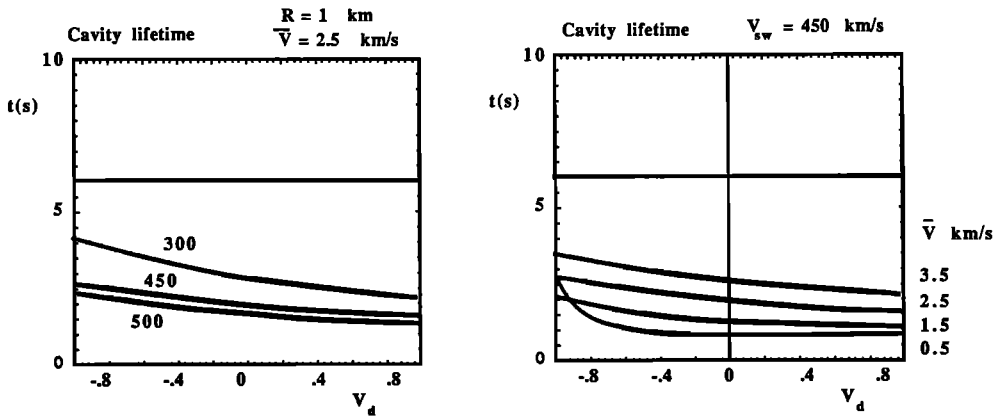

Fig. 8. This figure is in the same format as Figure 3 and refers to the September 20 lithium release.

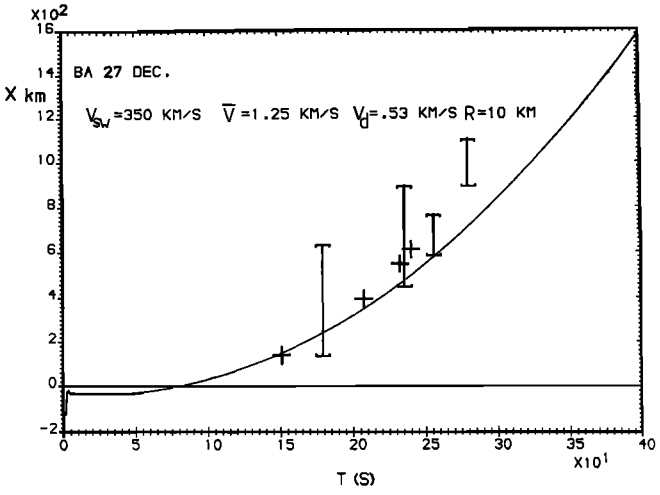

Fig. 9. This figure is a plot of the predicted snowplough displacement (from the IRM at x = 0) versus time, which has been calculated for the December 27 barium release, for typical parameters v_{sw} = 350 km s^{-1}, $\bar{v}$ = 1.25 km s^{-1}, v_d = 0.53 km s^{-1}, and R = 10 km, chosen to also yield a cavity lifetime that is consistent with observations (this point in parameter space is marked by the asterisk in Figure 3). The observed release ion cloud displacements for this event are also marked on the plot by crosses [Rees et al., 1986] and error bars [Valensuela et al., 1986].

Mendillo, private communication, 1988), although these results are as yet not sufficiently processed to allow the detailed quantitative comparison with the predictions of the snowplough equations that is to be attempted here for the December 27 release.

In order to compare the motion of the release ion cloud directly with the predicted snowplough trajectory, the displacement of the snowplough as a function of time has been plotted in Figure 9. This particular snowplough trajectory has been calculated by integrating the snowplough equations for typical values of the drift and expansion speeds of the release ion cloud and the disturbed oncoming proton flow, v_d = 0.53 km s^{-1}, $\bar{v}$ = 1.25 km s^{-1}, and v_{sw} = 350 km s^{-1}, which have also been chosen to give a cavity lifetime that is consistent with the IRM measurement for the event. The point in parameter space corresponding to this choice is marked by the asterisk in Figure 3. The assumption that is inherent in the comparison to be made here is that the snowplough displacement that is shown in the figure corresponds to the transverse displacement that is observed, requiring a suitable deflection in the oncoming solar wind flow. Given that this is the case, we can then mark the observed release ion cloud displacements seen by Rees et al. [1986] (crosses) and Valensuela et al. [1986] (error bars) directly on the plot. The bounds of the error bars correspond to the locations of the edges of release ion cloud images which were subject to artificial enlargement due to overexposure and hence must presumably enclose the location of the snowplough itself. It is then clear from the plot that for most times there is good agreement between the predicted and observed deflections. There are several possible reasons for the discrepancy between the observations and predictions at later times. First, in integrating the snowplough equations of motion, we have assumed a constant value for the oncoming proton flow speed, which will clearly not be the case. Also, the snowplough field structure which is required to accelerate the release ion cloud will ultimately be expected to collapse, other forces then becoming more significant. Finally, we have only considered here the release ion cloud acceleration that can be achieved directly from the ram pressure of the oncoming proton flow (via the enhancements in the electron and magnetic pressures that constitute the snowplough moving field structure). The net acceleration that could be produced by considering the curvature in the magnetic field that must, in some sense, become draped around the release ion cloud has not been discussed, as a consequence of the one-dimensionality of the simple model used here. The initial justification for these simplifications in the description presented here is based upon the uncertainties in the various parameters that are required to determine the snowplough motion. The extent to which the predictions of the simple model have been found to agree with the observations then supports the approach employed here.

4.3. Transverse Momentum Transfer

One further prediction of the simple snowplough model is required in order for the above interpretation of the optical observations to be consistent. It remains to be shown whether or not a sufficient proportion of the release population is photoionized upstream of the snowplough field structure to cause a substantial transverse deflection in the oncoming proton flow. This deflection in the oncoming flow is of course required in order to account for the transverse motion that is observed in the barium release ion clouds which we have assumed here are accelerated principally by the snowplough process. Since the integration of the snowplough equations of motion yields the snowplough location with respect to that of the release cloud at all times, it is straightforward to calculate the proportion of release neutrals which are photoionized upstream of the infinite planar membrane that is used to represent the snowplough. This calculation is three dimensional in the sense that the function for the neutral number density $f_{tot}(x,y,z,t)$ (equation (5)) (along with the assumptions implicit in (7) concerning the drift and expansion speeds of the cloud) that was derived in the previous section will be employed.

The photoionisation rate R_p per unit volume at any point in space and time is simply

$$R_p = N_o\, f_{tot}(x,y,z,t)\, \frac{e^{-t/\tau_p}}{\tau_p} \tag{11}$$

so that the fraction F of the total number of neutrals released that photoionize upstream of the snowplough location x_p between t - t + Δt is

$$F(t) = \frac{e^{-t/\tau_p}}{\pi\sqrt{\pi}(R^2 + \bar{v}^2t^2)^{3/2}}\, \frac{\Delta t}{\tau_p} \int_{-\infty}^{x_p} \exp-\left[\frac{(x - v_dt)^2}{R^2 + \bar{v}^2t^2}\right] dx \cdot \int_{-\infty}^{\infty} \exp-\left[\frac{y^2}{R^2 + \bar{v}^2t^2}\right] dy \int_{-\infty}^{\infty} \exp-\left[\frac{z^2}{R^2 + \bar{v}^2t^2}\right] dz \tag{12}$$

The integrals over y and z are just standard in form, so that (12) may be rewritten as:

$$F(t) = \frac{e^{-t/\tau_p}\Delta t}{\tau_p\sqrt{\pi}} \left[\frac{\sqrt{\pi}}{2} + \int_0^{u(x_p)} e^{-u^2} du\right] \tag{13}$$

where

$$u(x) = \frac{(x - v_d t)}{(R^2 + \bar{v}^2 t^2)^{\frac{1}{2}}}$$

so that when $x_p < v_d t$, the snowplough is located upstream of the center of the drifting Gaussian neutral cloud. Equation (13) was evaluated numerically at each time step during the integration of the snowplough equations of motion. The sum of the fraction F photoionized upstream at each time step then yields the total fraction photoionized upstream during the entire event. It was then found for both barium release events considered here that ~ 10–15% of the total number of neutrals released N_o are photoionized upstream of the snowplough. It is difficult to estimate the effect that this might have directly on the oncoming proton flow from simple considerations, principally due to the strong time dependence and two-dimensionality of the problem. However, since the proton population only acts as an intermediary in the transfer of transverse momentum between the snowploughed release ions and the release ions created upstream, we can still assess whether or not the observed transverse motion of the release ion cloud is predicted in a consistent way by our simple snowplough model.

Knowing the fraction of the total mass of release ions created upstream of the snowplough relates the (transverse) speed of this population v_u with that of the snowplough itself, i.e., $V_p \approx v_u/9$ by conservation of momentum. To make an estimate of the speed of the release ions in the upstream region v_u we can simply assume that they are accelerated in the ambient convection electric field $E_c \sim 5$ mV m^{-1}, which will represent an overestimate since the local convection electric field in the region of disturbed oncoming proton flow just upstream of the snowplough will be reduced due to the presence of the release ions themselves, but might be expected to be reasonable to within an order of magnitude. The momentum gained by the upstream release ions appropriate to this calculation is just that which they "pickup" while interacting with the oncoming protons that will subsequently transfer momentum to the snowploughed release ion cloud. This oncoming proton population must therefore be expected to be deflected over a region which has dimensions on the scale of the release cloud itself, i.e., on a scale $\Delta L \sim 100$ km. Given that this is the case, the "pickup" speed of the release ions upstream after traversing this distance is ~ 27 km s^{-1}, implying a snowplough speed of $V_p \sim 3$ km s^{-1}. This estimate is in good agreement with typical values of aproximately a few kilometers per second found from integrating the snowplough equations of motion, and given the approximations involved, it also compares favorably with the observed transverse velocity of the release ion cloud of ~ 5–6 km s^{-1} [Rees et al., 1986]. After $\Delta t \sim 250$ s, the time taken for significant transverse motion to be observed in the release ion cloud (see Figure 9), the snowplough displacement would be expected to be $\sim V_p \Delta t \sim 750$ km, which is in good agreement with the ~ 600–700 km that is actually observed at this time. The order of magnitude estimate above therefore suggests that the fraction of release ions that are found to be created upstream of the snowplough by integrating the simple snowplough equations of motion will be adequate to balance the observed transverse momentum of the release ion cloud, so that we are justified in equating the predicted displacements of the snowplough with the observed transverse displacement of the release ion clouds, as has been done in Figure 9.

5. Summary

In this paper we have presented the global effects of a simple mechanism by which the momentum of the oncoming solar wind or magnetosheath flow is transferred to the dense ion clouds that were produced during the early phases of the AMPTE lithium and barium releases. This process was suggested by the properties of the quasi-steady boundary layer structure that was found to form locally between the bulk of the release ions and the oncoming proton flow in the one-dimensional hybrid simulations of Chapman and Schwartz [1987] allowing momentum transfer to take place between the two populations. Here we have modeled this boundary layer by a simple planar moving membrane (a snowplough), which absorbs momentum from the oncoming protons, transferring it to the release ions which it encounters. As a result, this release ion population becomes gathered up by the snowplough fields as they propagate into the release ion cloud, so that ultimately the bulk of the release ions becomes associated with the snowplough itself. The direction of motion of the snowplough is just that of the oncoming proton flow, and since the latter is deflected from the direction of the ambient flow in the vicinity of the snowplough by the presence of release ions that were created outside of the diamagnetic cavity and upstream of the snowplough fields, this simple model is qualitatively consistent with the observed transverse motion of the barium release ion clouds. In this paper equations of motion of the snowplough have been integrated, using parameters appropriate for the particular conditions of the various AMPTE releases, in order to establish quantitatively whether or not the simple snowplough model is consistent with both the IRM in situ data and ground-based observations. The following properties have been shown:

1. The lifetime of the diamagnetic cavity as seen by the IRM, which in the simple description discussed here corresponds to the time taken for the snowploughed release ions to return to the IRM location after the initial expansion of the release cloud, is predicted from the results of integrating the snowplough equations, given the uncertainties in the various parameters which are needed to represent the initial release cloud.
2. The displacement of the snowplough calculated for typical values of the parameters appropriate for the first barium release is consistent with the magnitude of the transverse displacement of the release ion cloud that was actually found from ground-based observations.
3. The snowplough motion calculated for the barium releases has been used to determine the total number of neutrals that photoionize upstream of the snowplough, and which are required to deflect the oncoming proton flow. Simple estimates suggest that the ~ 10–15% which are found to be ionized upstream would be sufficient to balance the transverse momentum of the remainder of the release ions, which form the observed snowploughed release ion cloud, the deflected protons acting as an intermediary in the transfer of momentum between the two release ion populations.

Acknowledgments. The author would like to thank R. Treumann, R. Anderson, and O. Bauer for providing the AMPTE/IRM plasma wave instrument data used in section 2 and S. J. Schwartz for invaluable discussions concerning this work.

The editor thanks R. Roussel-Dupre and another referee for their assistance in evaluating this paper.

References

Bernhardt, P. A., R. A. Roussel-Dupre, M. B. Pongratz, G. Haerendel, A. Valensuela, D. A. Gurnett, and R. R. Anderson, Observations and theory of the AMPTE magnetotail barium releases, J. Geophys. Res., 92, 5777, 1987.

Brecht, S. H., and V. A. Thomas, Three-dimensional

simulation of an active magnetospheric release, J. Geophys. Res., 92, 2289, 1987.

Carlsten, J. L., Photoionization of barium clouds via the ^3D metastable levels, Planet. Space Sci., 23, 53, 1975.

Chapman, S. C., and M. W. Dunlop, Ordering of momentum transfer along V∧B in the AMPTE solar wind releases, J. Geophys. Res., 91, 8051, 1986.

Chapman, S. C., and S. J. Schwartz, One-dimensional hybrid simulations of boundary layer processes in the AMPTE solar wind lithium releases, J. Geophys. Res., 92, 11059, 1987.

Cheng A. F., Transverse deflection and dissipation of small plasma beams and clouds in magnetized media, J. Geophys. Res., 92, 55, 1987.

Dunlop, M. W., S. C. Chapman, W. Baumjohann, and H. Lühr, Boundary layer structures in the AMPTE solar wind releases (abstract), Eos Trans. AGU, 68, 1424, 1987.

Gurnett D. A., T. Z. Ma, R. R. Anderson, O. H. Bauer, G. Haerendel, B. Häusler, G. Paschmann, R. A. Treumann, H. C. Koons, R. Holzworth, and H. Lühr, Analysis and interpretation of the shocklike electrostatic noise observed during the AMPTE solar wind lithium releases, J. Geophys. Res., 91, 1301, 1986a.

Gurnett D. A., R. R. Anderson, T. Z. Ma, G. Haerendel, G. Paschmann, O. H. Bauer, R. A. Treumann, H. C. Koons, R. Holzworth, and H. Lühr, Waves and electric fields associated with the first AMPTE artificial comet, J. Geophys. Res., 91, 10,013, 1986b.

Haerendel, G., A. Valensuela, O. H. Bauer, M. Ertl, H. Föppl, K. -H. Kaiser, W. Lieb, J. Loidl, F. Melzner, B. Merz, H. Neuss, P. Parigger, E. Rieger, R. Schöning, J. Stöcker, E Wiezorrek, and E. Molina, The Li/Ba release experiments of the Ion Release Module, IEEE Trans. Geosci. Remote Sensing, 23, 253, 1985.

Haerendel G., G. Paschmann, W. Baumjohann, and C. W. Carlson, Dynamics of the artificial comet, Nature, 320(6064), 700, 1986.

Krimigis S. M., G. Haerendel, R. W. Mc Entire, G. Paschmann, and D. A. Bryant, The Active Magnetospheric Particle Tracer Explorers (AMPTE) program, Eos Trans. AGU, 63, 843, 1982.

Lühr H., D. J. Southwood, N. Klöcker, M. Acuña, B. Häusler, M. W. Dunlop, W. A. C. Mier-Jedrzejowicz, R. P. Rijnbeek, and M. Six, In situ magnetic field measurements during the AMPTE solar wind Li^+ releases, J. Geophys. Res., 91, 1261, 1986a.

Lühr H., D. J. Southwood, N. Klöcker, M. W. Dunlop, W. A. C. Mier-Jedrzejowicz, R. P. Rijnbeek, M. Six, B. Häusler, and M. Acuña, In-situ magnetic field measurements of the AMPTE artificial comet, Nature, 320(6064), 700, 1986b.

Lui A. T. Y., C. C. Goodrich, A. Menkofsky, and K. Papadopoulos, Early time interaction of lithium ions with the solar wind in the AMPTE mission, J. Geophys. Res., 91, 1333, 1986.

Papadopoulos K., and A. T. Y. Lui, On the initial motion of artificial comets in the AMPTE releases, Geophys. Res. Lett., 13, 925, 1986.

Rees D., T. J. Hallinan, H. C. Stenbaek-Nielson, M. Mendillo, and J. Baumgardner, Optical observations of the AMPTE artificial comet from the northern hemisphere, Nature(6064), 320, 700, 1986.

Valensuela A., G. Haerendel, H. Föppl, F. Melzner, H. Neuss, E. Rieger, J. Stöcker, O. Bauer, H. Höfner, and J. Loidl, The AMPTE artificial comet experiments, Nature, 320(6064), 700, 1986.

S. C. Chapman, School of Mathematical Sciences, Queen Mary College, Mile End Road, London E1 4NS, U.K.

(Recieved January 20, 1988;
revised August 29, 1988;
accepted August 29, 1988.)